PHYSICAL REVIEW C VOLUME 25, NUMBER 6 JUNE 1982

Double K-hole creation accompanying K-electron capture decay of ^{131}Cs

Y. Isozumi*
Radioisotope Research Center, Kyoto University, Kyoto, Japan

Ch. Briançon and R. J. Walen
Centre de Spectrométrie Nucléaire et de Spectrométrie de Masse, 91406 Orsay, France
(Received 21 December 1981)

Double K-hole creation has been studied in the electron-capture decay of ^{131}Cs by measuring hypersatellite K x rays emitted when the double vacancies of the K shell are filled. The complex K lines observed with a two-Ge-detector coincidence spectrometer show evidence of the hypersatellite $K\alpha$ and $K\beta$ lines. The double K-hole creation probability is determined: $(1.4\pm0.1)\times10^{-5}$ per K-capture event. This value, which does not agree with theoretical predictions, is discussed in detail. The intensity ratio of the $K\alpha_1$ to $K\alpha_2$ hypersatellites is found to be 1.5 ± 0.2. The intensity of internal bremsstrahlung photons accompanying the K-electron capture decay has also been reevaluated.

[RADIOACTIVITY ^{131}Cs (EC) ^{131}Xe; (K x ray) $\otimes$ (K x ray) coincidences measured by Ge detectors, double K-hole creation probability, hypersatellite energy shift, ratio $K\alpha_1^K/K\alpha_2^H$, associated internal bremsstrahlung intensity.]

I. INTRODUCTION

By capture of an atomic electron into the nucleus during the electron capture decay (EC), the nuclear charge is changed from Ze to $(Z-1)e$ and the stationary correlation between the absorbed electron and other atomic electrons suddenly vanishes. These changes of charge distribution in the atom give rise to electronic excitation to unoccupied bound states (shakeup, SU) or ejection into the continuum (shakeoff, SO). An interesting case is the K-electron SO or SU during K-EC decay, which produces an atom with a completely vacant K shell. Reviews of the phenomenon have been given by several authors.[1–3]

The phenomenon was first studied theoretically by Primakoff and Porter[4] in 1963, using nonrelativistic variational wave functions for two K-shell electrons in the parent atom. A different method for constructing the initial two electron wave function was introduced by Intemann and Pollock,[5] according to the Glauber-Martin formulation with Coulomb Green's functions.[6] Intemann developed the method and performed a series of calculations to predict the SO probability and the ejected electron spectrum.[7,8] In his relativistic calculation, the symmetric wave functions of Biedenharn and Swamy[9] were employed as an approximation for computational simplifications. Law and Campbell[10] used a formulation different from that of Intemann which is similar to a technique used by Paquette[11] for summing the eigenfunction expansion of the Coulomb Green's function over discrete and continuum states. However, the expansion was cut off at too low an order to obtain reliable results, as pointed out by Intemann.[8]

Stephas[12] used the same overlap integral that was introduced to estimate the SO probability during β decay. The complete calculation with an overlap integral is owing to Mukoyama *et al.* (MIKS).[13] The screening constants used were determined separately from relativistic self-consistent-field (SCF) calculations, to take into account the electron-electron interaction in the initial state. The total K-SO probability agrees fairly well with Intemann's calculations.

Experiments on double K vacancy are difficult because of the small probability of occurrence, viz., of the order of $10^{-4}-10^{-5}$ per K capture. Events are generally obscured by the background resulting from both the Compton tail of the γ rays and the K x rays associated with the corresponding internal conversion. Therefore, measurements can only be performed when the EC transition leads to the ground state of the daughter nucleus or to a metastable state with an excitation energy less than the

K-binding energy of the daughter atom, unless internal conversion is negligible. Such cases are very rare; seven nuclides (^{7}Be, ^{37}Ar, ^{55}Fe, ^{71}Ge, ^{103}Pd, ^{131}Cs, and ^{165}Er) were studied in previous works. The determination of the double K-hole creation probability per K capture, P_{KK}, relies usually on measurements of the K x rays associated with the filling of the empty K shell. The first emitted K x rays are called hypersatellite lines denoted by α^H and β^H corresponding to the transitions ($K^{-2}\rightarrow K^{-1}L^{-1}$) and ($K^{-2}\rightarrow K^{-1}M^{-1}$ or $K^{-1}N^{-1}$), respectively. The next emitted K x rays are satellite lines, e.g., α^S ($K^{-1}L^{-1}\rightarrow L^{-2}$), β^S ($K^{-1}L^{-1}\rightarrow M^{-1}L^{-1}$ or $N^{-1}L^{-1}$), $\alpha^{S'}$ ($K^{-1}M^{-1}\rightarrow L^{-1}M^{-1}$), and $\beta^{S'}$ ($K^{-1}M^{-1}\rightarrow M^{-2}$ and $K^{-1}N^{-1}\rightarrow M^{-1}N^{-1}$). Satellite and hypersatellite lines are shifted in energy with respect to diagram lines. As we shall see in Sec. III, more complicated processes of atomic neutralization can also take place.

In 1960, Lark and Perlman[14] measured K x ray $\otimes$ K x ray coincidences with two NaI(Tl) crystals to determine the P_{KK} probability in the decay of ^{131}Cs. Nagy, Schupp, and Hurst[15] performed a similar measurement for the case of ^{131}Cs and ^{165}Er, using Si(Li) and NaI(Tl) detectors. In both groups, the α^H line could not be resolved from the diagram line because of insufficient energy resolution. von Oertzen[16] studied ^{71}Ge with a bent-crystal diffraction spectrometer and observed a satellite peak, probably due to the transition of ($K^{-1}L^{-2}\rightarrow L^{-3}$). The energy shift of the α^H line is about 300 eV for Ni and more than 1 keV for high Z elements above Pb. This is enough to observe the α^H line using high-resolution detectors. With such detectors, Briand *et al.*[17] observed the α^H line in coincidence with the corresponding α^S rays in the case of ^{71}Ge decay. With the same coincidence technique, van Eijk, Wijnhorst, and Popelier have determined the P_{KK} value for the EC decays of ^{103}Pd and ^{109}Cd.[18]

Some groups have studied the ejected electron spectrum through direct electron spectrometry,[19–23] but this has not lead unambiguously to the P_{KK} probability, because assumptions on the spectrum shape were needed. A pure K-SO electron spectrum was first observed by Kitahara and Shimizu,[24] who measured triple coincidences $X\otimes X\otimes e^-$ in the EC decay of ^{55}Fe. Neumann has recently succeeded in measuring a composite electron spectrum owing to K-SU/SO in K-EC decay, L-SO in K-EC, and K-SO in L-EC by means of internal-source counting of ^{37}Ar in a multiwire proportional counter.[25]

In spite of this extensive set of measurements and theoretical calculations, the large discrepancy between the experimental P_{KK} values together with approximations in the calculations still make it difficult to quantitatively discuss the phenomenon. In the present paper, we report on our x ray-x ray coincidence measurements, which yield a P_{KK} probability reliable enough to be compared with calculations. For our study, we choose ^{131}Cs, because (i) the decay takes place uniquely to the ground state, (ii) the technique for preparing high-purity carrier free sources is well established, and (iii) the predicted energy shift of the α^H line ($\sim$650 eV) is large enough to be observed directly with a high-resolution detector. In Sec. II, the experimental procedure is described. Section III explains the analysis of data used to deduce the P_{KK} probability, the intensity ratio of α_1^H to α_2^H lines, and the internal bremsstrahlung intensity. The comparison of our result of P_{KK} with previous calculations and some suggestions for future work are given in Sec. IV.

II. EXPERIMENTAL PROCEDURE

A. Source preparation

^{131}Cs results from the EC decay of ^{131}Ba obtained by (n,γ) reaction on the low-abundance (0.13%) isotope ^{130}Ba of natural barium. Since many undesired isotopes are produced by the irradiation of barium, they had to be carefully eliminated, e.g., ^{131}Ba (11.5 d) itself, ^{132}Cs (6.5 d) owing to ^{132}Ba (n,p), and ^{134}Cs (2.1 y) owing to ^{134}Ba (n,p). Therefore, the sample of 0.5 g natural "specpure" $Ba(NO_3)_2$ was irradiated at Saclay at a pile position where the fast-neutron flux was $<1\%$.

The source was then prepared in four steps: (i) complete removal of Cs from the irradiated sample, (ii) a period of growth of ^{131}Cs in the sample, (iii) extraction of Cs and elimination of Ba residues, and (iv) selective vacuum volatilization of Cs. Step 1 was achieved by repeated precipitation of $BaCl_2$ in concentrated HCl, adsorption on a large Dowex 50W-H^+ column (10 mm diam $\times$120 mm), and elution of Cs with 0.5N HCl. The column was left untouched for one week for step 2, being followed by step 3, i.e., elution of Cs with 1N NCl. The high purity is obtained by selective adsorption and elution on Dowex 50 columns of decreasing dimensions: 2 mm diam $\times$70 mm and 0.3 mm diam $\times$15 mm.[26] The carrier-free ^{131}Cs about 0.6 mCi, was obtained in 1 drop of 1N HCl, transformed to nitrate, dried in a platinum boat, and volatilized in

high vacuum at 1000°C onto a thin aluminum backing. This last step is also very selective because BaO volatilizes only at higher temperature.

Because the radiochemical purity is essential in this experiment, the ratio of contaminant activity to EC decay has been measured by means of high-statistics γ spectrometry. For ^{132}Cs and ^{131}Ba, upper limits are found to be 10^{-6} and 10^{-7} disintegrations per K capture of ^{131}Cs, respectively. The same measurements show that, taking into account known internal-conversion data, the feeding of the 80 keV level of ^{131}Xe is less than 3×10^{-8} per K capture, ensuring that this branching will not contribute notably to the K x ray $\otimes$ K x ray coincidence rates.

B. Coincidence measurements

The experimental layout for the present coincidence measurements is shown schematically in Fig. 1. The 0.01 mm thick aluminum foil with evaporated ^{131}Cs was cut into pieces of 0.3×0.2 mm^2. A piece with an activity of about 1 μCi was mounted in the middle of the central hole (1 mm in diameter) of an aluminum foil, which was then sandwiched between two 2 mm thick tantalum diaphragms with 1 mm diameter tapered holes. The diaphragms were fixed between the two detectors to give maximum detector efficiency. Electrons and low-energy photons were absorbed by 50 μm thick aluminum foils. Two planar Ge detectors were used to detect x rays from the ^{131}Cs source; the one with a better energy resolution (FWHM: 420 eV for 30 keV photons) is a pure Ge crystal of 4 cm$^2\times7$ mm.

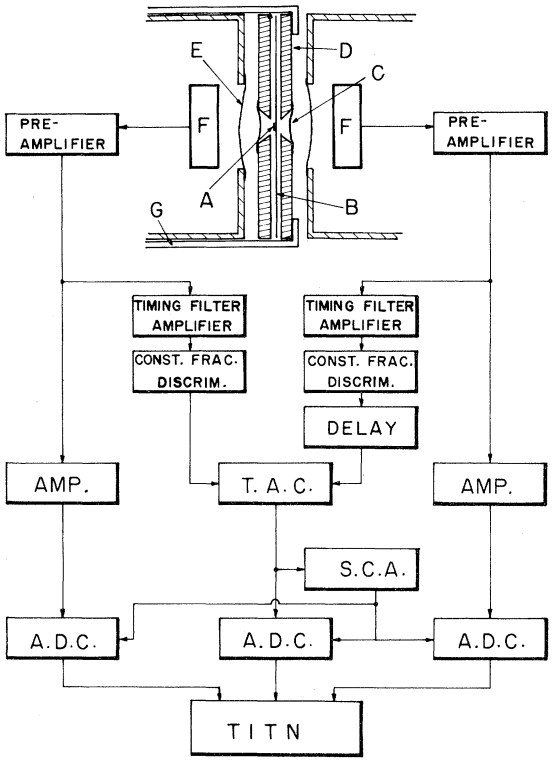

FIG. 1. Experimental arrangement and electronic system used in the present coincidence measurement: A, ^{131}Cs source; B, disk (25 μm thick aluminum foil); C, absorber (50 μm thick aluminum foil); D, diaphram (2 mm thick tantalum plate with tapered hole); E, beryllium window; F, Ge crystal.

A conventional fast-slow coincidence system was used for the measurements. The data obtained were stored on a magnetic tape. The coded data were the photon energies E_1 and E_2, and the time interval $t(=t_1-t_2)$. The maximum time interval stored was adjusted to about 500 nsec. All events on the magnetic tape were classified by the IBM 370 of the data processing computer ARIEL of Orsay. The time resolution of the system was about 30 nsec, deduced from a time spectrum measured with coincident K x ray pairs from ^{133}Ba.

During 115 d, two separate measurements were performed with a low counting rate of 400 to 800/sec. Overall stability of the electronics was about 10^{-4}, ensured by a constant-temperature shielded room. The drift of peak position was less than 15 eV with daily testing of the peak position.

In Fig. 2, we show as an example the result of the second measurement, which has better statistics; RT is the spectrum observed by the pure Ge detector in coincidence with Xe K x rays detected by the other detector and the corresponding random coincidence spectrum is given by R. Two bumps appear on the spectrum RT: a $K\alpha$ hypersatellite ($\alpha_1^H+\alpha_2^H$) on the high energy side of the $K\alpha$ diagram line and a $K\beta_2$ hypersatellite on the high-energy side of the $K\beta_2$ diagram line. The hypersatellite $K\beta_{1,3}$ line cannot be observed in the spectrum RT, since it is superimposed on the diagram $K\beta_2$ line. The true coincidence spectrum denoted by T is obtained by the subtraction ($RT-R$). The spectrum F corresponds to unwanted coincidences owing to Xe K x rays $\otimes$ internal bremsstrahlung (IB) and Xe K x rays $\otimes$ Compton tail of Ta K x rays as explained in the next section.

III. DATA ANALYSIS

In order to determine the double K-hole creation probability per K capture, P_{KK}, it is necessary to ex-

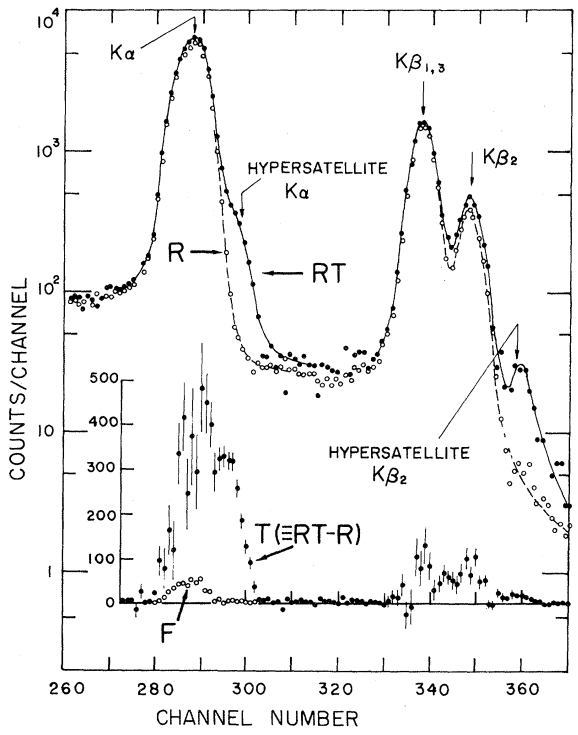

FIG. 2. Typical experimental coincidence spectra: RT, photon spectrum observed by the pure Ge detector in coincidence with Xe K x ray detected by the second Ge detector; R, corresponding random coincidence spectrum; $T(\equiv RT-R)$, true coincidence spectrum obtained by subtracting the spectrum R from the spectrum RT; F, unwanted coincidence spectrum caused by coincidences between Xe K x rays and IB photons and between Xe K x rays and the Compton tail of Ta K x rays.

tract the net count N_H owing to hypersatellites $(\alpha_1^H+\alpha_2^H)$ in the coincidence spectrum RT or $T(\equiv RT-R)$. The N_H counts have been deduced from two independent methods. Firstly, the $T(\equiv RT-R)$ spectrum has been carefully analyzed taking account of possible unwanted counts determined experimentally. Secondly, the $K\alpha$ peaks in both RT and $T(\equiv RT-R)$ spectra have been decomposed into individual K lines by means of nonlinear least-squares fits. We have found good agreement between the N_H counts by both methods.

A. Unwanted counts in the $T(\equiv RT-R)$ spectrum

The following coincidence processes mainly contribute to the $K\alpha$ peak of the measured $T(\equiv RT-R)$ spectrum: (i) Xe K x ray $\otimes$ Xe K x ray during the neutralization of the double K-hole initial state, (ii) Xe K x ray $\otimes$ IB (internal bremsstrahlung) accompanying the EC decay, and (iii) Xe K x ray $\otimes$ Ta K x ray due to interaction of high-energy IB photons with the Ta diaphragms (D in Fig. 1). Coincidences due to the processes (ii) and (iii) are called unwanted counts in the present measurement.

In order to examine a contribution of process (ii), coincidences between photons with energies of 70.0→86.0 keV detected by the pure Ge detector, D_1, and Xe K x rays (27.7→35.6 keV) detected by the other detector, D_2, have been registered. The spectrum in the 70→86 keV region is entirely due to IB photons with no detectible traces of Ta K x rays and pileup signals. The coincidence count $N_{\rm IB}$ between K x rays and IB photons is

$$N_{\rm IB}=N_0\cdot\rho_{\rm IB}(70.0\rightarrow 86.0)\cdot P_{\rm IB}\cdot\omega_K \times\epsilon_1(70.0\rightarrow 86.0)\cdot\epsilon_2(27.7\rightarrow 35.6)\,, \quad (1)$$

while the total $K\alpha$ count N_α in the $T(=RT-R)$ spectrum is given by

$$N_\alpha=2\cdot N_0\cdot P_{KK}\cdot\omega_{K\alpha}\omega_K\cdot\epsilon_1(28.8\rightarrow 33.3) \times\epsilon_2(27.7\rightarrow 35.6)\,, \quad (2)$$

where, respectively, N_0 is the number of atoms undergoing EC decay, and P_{KK} and $P_{\rm IB}$ are the total double K-hole creation and IB emission probabilities per K-capture decay. The quantity $\rho_{\rm IB}(70.0\rightarrow 86.0)$ is the relative intensity of IB photons in the region of 70→86 keV. The factors $\epsilon_1(E)$ and $\epsilon_2(E)$ are the overall detection efficiencies of the D_1 and D_2 detectors for the photon energy ranges indicated in parentheses. The factors ω_K (=0.904) (Ref. 27) and $\omega_{K\alpha}$ (=0.73) (Ref. 28) are the fluorescence yields for total K x rays and $K\alpha$ x rays, respectively. From the spectra obtained in the second run, $N_{\rm IB}$ and N_α have been estimated to be 650 and 5787, respectively. A value for $\rho_{\rm IB}(70.0\rightarrow 86.0)$ has been estimated from the shape of the spectrum of ^1s IB photons measured by Biavati, Nassiff, and Wu (BNW) (Ref. 29): $\rho_{\rm IB}(70.0\rightarrow 86.0)\simeq 0.09$. Neglecting a small difference between $\epsilon_1(28.8\rightarrow 31.3)$ and $\epsilon_1(70.0\rightarrow 86.0)$, we obtain

$$P_{\rm IB}\simeq 1.8P_{KK}\,. \quad (3)$$

Using the present result of $P_{KK}(=1.4\times 10^{-5})$, as explained below, the IB emission probability $P_{\rm IB}$ has been deduced to be $(2.5\pm 0.7)\times 10^{-5}$, in which the error has been estimated rather conservatively.

This is to be compared with the value of $(1.4\pm1.0)\times10^{-5}$ measured by BNW.

Coincidences between photons in the region of 38.6→46.5 keV and Xe K x rays have also been counted to examine the effect of a possible contribution from process (iii). Photons in the 38.6→46.5 keV region consist of IB photons, the Compton tail of Ta K x rays, and pileup signals owing to the predominant intensity of diagram Xe K x rays. Since pileup signals do not coincide with Xe $K\alpha$ x rays, the total coincidence count $N_{\mathrm{IB+Ta}}$ (552 counts) originates from the IB photons and the Ta K x-ray Compton tail. The ratio of $N_{\mathrm{IB+Ta}}$ to the total $K\alpha$ count N_α in the $T(\equiv RT-R)$ spectrum is given by

$$\frac{N_{\mathrm{IB+Ta}}}{N_\alpha}=\frac{1}{2}\rho_{\mathrm{IB}}(38.6\rightarrow46.5)\frac{P_{\mathrm{IB}}}{P_{KK}}(1+\Delta)\times\frac{1}{\omega_{K\alpha}}\frac{\epsilon_1(38.6\rightarrow46.5)}{\epsilon_1(28.8\rightarrow31.3)}\ . \tag{4}$$

The factor $\rho_{\mathrm{IB}}(38.6\rightarrow46.5)$ is estimated to be 0.03 from Fig. 13 of Ref. 29 and Δ is a factor indicating the contribution of the Ta K x rays to the $N_{\mathrm{IB+Ta}}$ count. Using Eq. (3) and neglecting a slight difference between $\epsilon_1(28.8\rightarrow31.3)$ and $\epsilon_1(38.6\rightarrow46.5)$, we obtain $\Delta\simeq1.5$ which means that the contribution due to Ta K x ray to the coincidence count $N_{\mathrm{IB+Ta}}$ is about 1.5 times that due to the IB photons. Thus, it is expected that the true coincidence spectrum $T(=RT-R)$ contains a non-negligible amount of unwanted events. An unwanted coincidence spectrum obtained by the second measurement is shown Fig. 2 (curve F). This represents the Xe $K\alpha$ x rays detected by D_1 in coincidence with 38.4→46.7 keV photons detected by D_2 whose energies are slightly higher than those used in constructing the $T(\equiv RT-R)$ spectrum, i.e., 27.7→35.6 keV. The true coincidences due to process (i) for the second measurement have been evaluated as

$$N_T=N_\alpha-N_f-N_{\mathrm{Comp}}=5332\pm280\ , \tag{5}$$

where $N_f(=399\pm100)$ is the total count of the unwanted coincidence peak F and $N_{\mathrm{Comp}}(=156\pm50)$ is the estimated contribution from the Compton tail of $K\beta$ x ray peaks. Since the count due to $K\alpha$ hypersatellite lines, N_H, is one half of N_T, we obtain

$$N_H=2616\pm140\ , \tag{6}$$

for the second measurement, described above.

B. Analysis of the $T(\equiv RT-R)$ spectrum

The $T(\equiv RT-R)$ spectrum has been analyzed taking into account calculated energies of electronic transitions in the presence of spectator vacancies, as well as probable predictions of the intensities of the different paths by which a K^{-2} atom will be neutralized.

1. X-ray energies

The unfolding of the spectra is very complicated, because many line components are contributing: (i) diagram lines denoted by α_1^N and α_2^N; (ii) satellites due to $(K^{-1}M^{-1}\rightarrow L^{-1}M^{-1})$ and $(K^{-1}N^{-1}\rightarrow L^{-1}N^{-1})$ transitions, $\alpha_1^{S'}$ and $\alpha_2^{S'}$; (iii) satellites due to $(K^{-1}L^{-1}\rightarrow L^{-2})$, α_1^S, and α_2^S; and (iv) hypersatellites due to $(K^{-2}\rightarrow K^{-1}L^{-1})$, α_1^H, and α_2^H. Neglecting a small difference in energy between α^N and $\alpha^{S'}$ lines, it has been assumed that there exist six components in the $K\alpha$ peak, i.e., $\alpha_1^{N+S'}$, $\alpha_2^{N+S'}$, α_1^S, α_2^S, α_1^H, and α_2^H. We have calculated the energy shifts between satellite and hypersatellite lines, and diagram lines, with the aid of the multiconfiguration Dirac-Fock (MCDF) code of Desclaux,[30,31] for which we verified extensively that one-hole and two-hole configuration energy predictions are excellent. Results of the shifts and energies of individual $K\alpha$ lines are listed in Table I.

2. Relative intensities of the $K\alpha$ lines

The different paths for the decay of the double K-hole state are shown in Fig. 3. The relative intensities of $\alpha^{N+S'}$, α^S, and α^H lines in coincidence with both $K\alpha$ and $K\beta$ x rays have been deduced using emission rates of diagram lines roughly estimated for x-ray line widths:

$$I(\alpha^H):I(\alpha^S):I(\alpha^{N+S'})=0.50:0.34:0.16\ . \tag{7}$$

Taking account of the extra α^N contribution due to unwanted coincidences, i.e., Xe K x ray ⊗ IB and Xe K x ray ⊗ Ta K x ray Compton tail, the relative intensities of $K\alpha$ components in the $T(\equiv RT-R)$ spectrum are predicted as

$$I(\alpha^H):I(\alpha^S):I(\alpha^{N+S'})=0.46:0.32:0.22\ . \tag{8}$$

The $K\alpha_1/K\alpha_2$ intensity ratios used in the analysis are

TABLE I. Energies of Xe $K\alpha$ x rays.

$K\alpha$ x ray component	Transition	State	Energy shift[b] (eV)	Energy (eV)
α_1^N				29779±2[a]
α_2^N				29458±2[a]
α_1^H	$S(1s;2p\rightarrow 1s)$	$^3P_1$	644±10	30423±10
α_2^H	$S(1s;2p^*\rightarrow 1s)$	$^1P_1$	631±10	30089±10
α_1^S	$S(2p^*;2p\rightarrow 1s)$	$^1P_1$	67±20[c]	29846±20
	$S(2p;2p\rightarrow 1s)$	$^3P_1$		
α_2^S	$S(2p^*;2p^*\rightarrow 1s)$	$^1P_1$	65±20[c]	29523±20
	$S(2p;2p^*\rightarrow 1s)$	$^3P_1$		

[a]Quoted from J. A. Bearden, Rev. Mod. Phys. 39, 78 (1967).
[b]Present calculations by the MCDF code. Probable errors in the calculation are ~10 eV.
[c]Average value of various components.

$$\rho_{N+S'}[I(\alpha_1^{N+S'})/I(\alpha_2^{N+S'})]=1.85\ , \tag{9}$$

$$\rho_S[I(\alpha_1^S)/I(\alpha_2^S)]=2.0\ , \tag{10}$$

and

$$\rho_H[I(\alpha_1^H)/I(\alpha_2^H)]=1.56\ . \tag{11}$$

Here the value of $\rho_{N+S'}(\simeq\rho_N)$ is taken from Scofield.[28] The ρ_H value was first evaluated by Åberg *et al.*,[32] then calculated by us with the MCDF code, and this value (1.56) was confirmed by Åberg and Suvanen[33] in systematics of ρ_H. These calculations agree with $\rho_H=1.5\pm0.2$ resulting from our least-squares-fit analysis given below. Since no one has so far evaluated a value for ρ_S, we have employed a value of 2.0 based on some simplifying assumptions.

3. *Decomposition of the* $T(=RT-R)$ *spectrum*

In order to obtain a single line profile, the $K\alpha$ peak of the random coincidence spectrum R has been separated in the components $K\alpha_1$ and $K\alpha_2$ by a method of successive subtractions. The difference

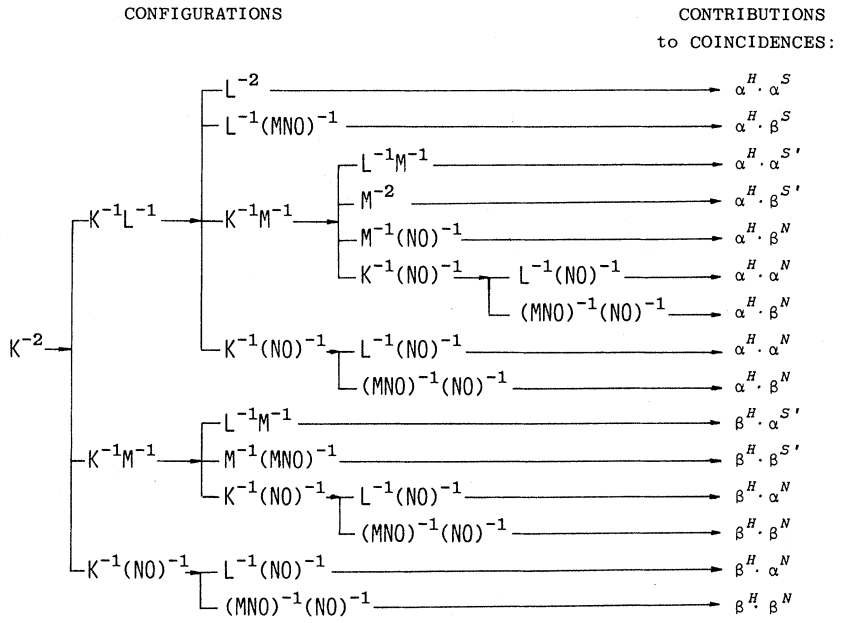

FIG. 3. Different paths for the decay of the double K-hole (K^{-2}) state contributing to the K x ray - K x ray coincidences.

of the peak positions $\Delta X(\equiv X_{\alpha_1}-X_{\alpha_2})$ was fixed at 321 eV in this deconvolution. With the ratio $\rho_N[\equiv I(\alpha_1^N)/(\alpha_2^N)]$ taken as a parameter, a best fit was obtained for $\rho_N=1.85$ in good agreement with theoretical predictions and systematics. The background was assumed to be a straight line and was subtracted from the original data.

Using the decomposed line profile and the intensity ratios of Eqs. (9)–(11), and fixing the position of each line at the value predicted by the MCDF calculations, the coincidence spectrum $T(=RT-R)$ has been calculated, as shown in Fig. 4. The agreement between experimental data and the composed spectrum is satisfactory:

$$\chi^2=\frac{1}{n}\sum_{i=1}^{n}\left[\frac{F_i-M_i}{\Delta M_i}\right]^2=0.95\ , \tag{12}$$

where n is the number of data points, M_i is the measured counting rate at the point i, ΔM_i is the probable error of M_i, and F_i is the counting rate at the point i in the estimated complex spectrum.

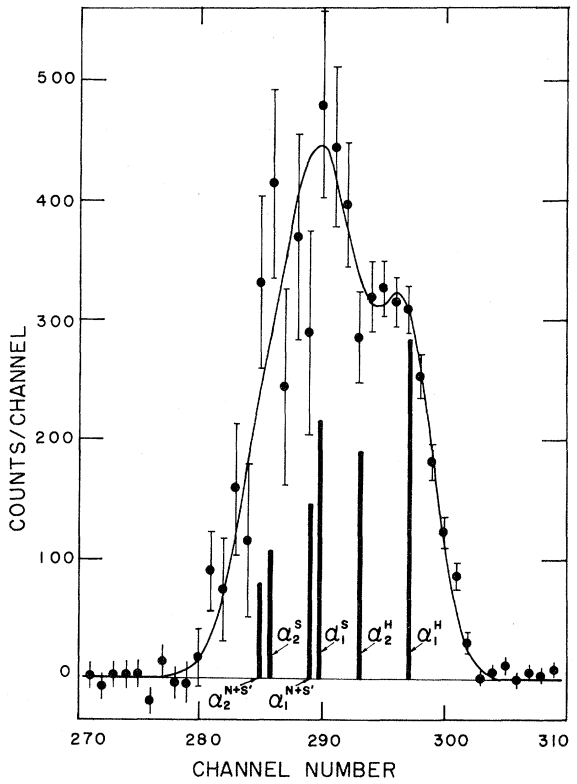

FIG. 4. Composite K peak in the $T(\equiv RT-R)$ spectrum. Continuum background is subtracted from the original data, i.e., $T(\equiv RT-R)$ spectrum in Fig. 2. The solid curve has been obtained by summing of the $\alpha_2^{N+S'}$ (7.7%), α_2^S (10.5%), $\alpha_1^{N+S'}$ (14.3%), α_1^S (21.1%) α_2^H (18.6%), and α_1^H (27.8%) lines.

C. Nonlinear least-squares fit

The $K\alpha$ peaks in both RT and $T(\equiv RT-R)$ spectra have been systematically decomposed into individual x-ray lines by means of nonlinear least-squares fits. Since the measured spectra are too complicated, we have been obliged to employ some reasonable constraints in order to decrease the number of free parameters in the fitting. A special code of the χ^2 fit with linear constraints has been prepared for the present analysis with the FACOM M190 computer of the Data Processing Center of Kyoto Univeristy by one of us (Y.I.).

The following assumptions have been used in the fit:

(i) It is assumed that there exist six lines in the $K\alpha$ peaks of RT and $T(\equiv RT-R)$ spectra, i.e., $\alpha_1^{N+S'}$, $\alpha_2^{N+S'}$, α_1^S, α_2^S, α_1^H, and α_2^H lines.

(ii) A pure Gaussian line profile was determined by an independent fit to the $K\alpha(\equiv\alpha_1^N+\alpha_2^N)$ peak in the random coincidence spectrum R. We have found that this line profile agreed satisfactorily with the result of the successive subtraction method.

(iii) The peak width, mainly originating from the detector, is assumed to be the same for the six components.

(iv) The background continuum has been taken as a straight line. Peak positions of the six lines have been fixed at the values predicted by the MCDF calculation. The necessary calibration between x-ray energy and peak position has been performed by use of x-ray sources of ^{131}Cs and ^{133}Ba.

Important and interesting quantities to be deduced from the fits are the total count of $K\alpha$ hypersatellites, N_H, and the α_1^H/α_2^H ratio, ρ_H. These quantities deduced from data obtained by the second measurement are shown in Fig. 5(a) and (b). Bars in the figure indicate probable errors, which were evaluated by use of the covariance matrix for free parameters determined by the fits. The details of each fit are presented briefly:

(i) Fit I. Variable parameters are peak heights of the six lines.

(ii) Fit II. The intensity ratio $\rho^{N+S'}$ $[\equiv I(\alpha_1^{N+S'})/I(\alpha_2^{N+S'})]$ is fixed at 1.85.

(iii) Fit III. The intensity ratio of $K\alpha$ satellite to $K\alpha$ hypersatellite, denoted by $\rho_{S/H}$, is fixed in this fit:

$$\rho_{S/H}=[I(\alpha_1^S)+I(\alpha_2^S)]/[I(\alpha_1^H+I(\alpha_2^H)]\ . \tag{13}$$

The most probable value of $\rho_{S/H}$ is deduced to be 0.70 from Eq. (8). Results for N_H and ρ_H in the

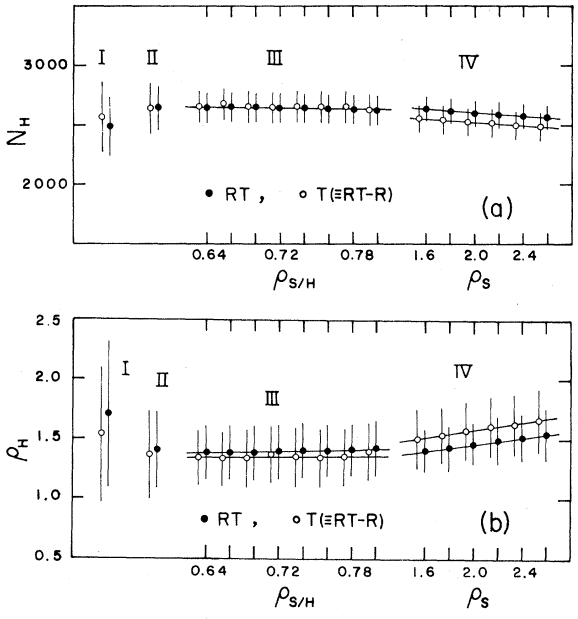

FIG. 5. Results of the nonlinear least-squares fit with constraints: (a), total hypersatellite count N_H; (b), α_1^H/α_2^H ratio ρ_H.

range of $\rho_{S/H}=0.64\rightarrow 0.84$ are shown in Fig. 5 (a)-III and (b)-III, respectively. Both N_H and ρ_H do not depend very much on $\rho_{S/H}$.

(iv) Fit IV. With the results of fit II, a α_1^S/α_2^S ratio, ρ_S, is estimated to be (1.5 ± 0.8) and (0.8 ± 0.4) for the RT and $T(\equiv RT-R)$ spectra, respectively. Since (0.8 ± 0.4) is obviously too small, this ratio is fixed at a reasonable value of fit IV. The ratio $\rho_{S/H}$ is also fixed at the most probable value of 0.7. Results in the range of $\rho_S=1.6\rightarrow 2.6$ are shown in Fig. 5 (a)-IV and (b)-IV, respectively. The ρ_H is enhanced by this constraint while N_H is decreased a little.

In order to determine N_H and ρ_H from the figure, it is assumed that the possible values of ρ_S extend from 1.6 to 2.4. Determined values of N_H and ρ_H with probable errors are listed in Tables II and III, respectively. All the results from the RT and

TABLE II. $K\alpha$ hypersatellite intensity $N_H[\equiv I(\alpha_1^H)+I(\alpha_2^H)]$.

Spectrum	First measurement	Second measurement
RT	1430±100	2590±140
$T(\equiv RT-R)$	1420±100	2520±150
		2620±140[a]

[a]Value determined after separate substraction of unwanted counts (see Sec. III A).

TABLE III. Intensity ratio $\rho_H[\equiv I(\alpha_1^H)/I(\alpha_2^H)]$.

Spectrum	First measurement	Second measurement	Weighted average
RT	1.56±0.31	1.47±0.24	1.50±0.19
$T(\equiv RT-R)$	1.48±0.37	1.58±0.30	1.54±0.23

$T(\equiv RT-R)$ spectra are satisfactorily consistent with each other. Note that the N_H value from the $T(\equiv RT-R)$ spectrum by the second measurement is in good agreement with the value determined by the independent method explained in Sec. III A. Present fits of $T(\equiv RT-R)$ spectra indicate that $K\alpha(\equiv\alpha^N+\alpha^N)$ diagram lines have a relative intensity of $(12\pm 6)\%$, which agrees well with the conclusion obtained in Sec. III A; the $K\alpha$ peak in the $T(\equiv RT-R)$ spectrum contains about 7% of $K\alpha$ diagram lines due to unwanted coincidences, i.e., Xe $K\alpha$ x rays ⊗ IB photons and Xe $K\alpha$ x rays ⊗ Ta K x Compton tail.

The final result for the α_1^H/α_2^H ratio is

$$\rho_H=1.5\pm 0.2 \tag{14}$$

and agrees with the theoretical prediction of 1.56, mentioned above (Sec. III B 1).

D. Double K-hole creation probability per K capture

The total double K-hole creation probability per K capture, P_{KK}, is given by the equation:

$$P_{KK}=\frac{\omega_K}{\omega_K^H\omega_K^S}\frac{N_H}{\epsilon_c}\frac{1}{R_\alpha}\frac{1}{\delta}, \tag{15}$$

where

$$\delta=\epsilon_1\sum_{i=1}^{n}\frac{1-e^{-\lambda\Delta T_i}}{\lambda}n_{D1}^i(0), \tag{16}$$

$$=\epsilon_2\sum_{i=1}^{n}\frac{1-e^{-\lambda\Delta T_i}}{\lambda}n_{D2}^i(0). \tag{17}$$

Here ω_K, ω_K^S, and ω_K^H are the fluorescence yields for diagram, satellite, and hypersatellite K lines, respectively. The fluorescence yields of a doubly ionized atom have approximately the same value as that of a singly ionized atom, i.e., $\omega_K^H\sim\omega_K^S\sim\omega_K=0.904$.[27] The factor N_H is the total count of $K\alpha$ hypersatellite rays during the coincidence experiment. The ratio $R_\alpha=\alpha^H/\alpha^H+\beta^H$ was deduced from the

$T(=RT-R)$ spectrum in Fig. 2, which agrees well with the theoretical prediction for diagram lines: $R_\alpha \simeq 0.81$.[28]

The factor ϵ_C is the coincidence efficiency, in which real coincidence events are accepted by the present experimental system. To estimate this value, we used the time spectrum obtained by classifying the original data in the magnetic tape, as shown by Fig. 6 (a). Random coincidence counts under the true coincidence peak are indicated by a straight line, which is an average of counts from channel 200 to 500. Then, the coincidence efficiency with a time interval Δt is defined as the ratio $N(\Delta T)/N$, where N and $N(\Delta t)$ are the total count in the coincidence peak and the sum of counts in the region Δt of the peak. These factors have been deduced from a smoothed integrated time spectrum shown in Fig. 6 (b). Corresponding to the actual time interval from 60 to 109 channels, the efficiency ϵ_c is determined to be 0.92 for both first and second measurements.

In Eqs. (16) and (17), λ is the decay constant of ^{131}Cs for which we adopted $(8.28\pm0.04)\times10^{-7}$/sec.[14] The overall detection efficiencies ϵ_1 and ϵ_2 of the two Ge detectors for Xe K x rays have been determined with a ^{131}Cs source, carefully calibrated in the Laboratoire de Métrologie des Rayonnements Ionisants (CEN Saclay) to within an uncertainty of 2% by two independent methods: a specially calibrated NaI(T1) counting system and a pressurized proportional counter filled with argon gas. The factors $n^i_{D1}(0)$ and $n^i_{D2}(0)$ are the initial count rates of the pure Ge and the second Ge detectors, respectively. Because of the ^{131}Cs half-life of 9.7 days, the source was changed once a week in order to maintain a counting rate of 800→400 c/sec. The δ in Eq. (15) has been determined from a weighted average of values deduced from Eqs. (16) and (17).

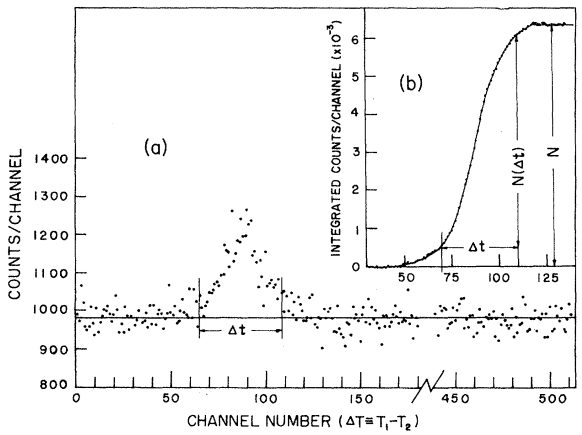

FIG. 6. Time spectrum used to determine the coincidence efficiency ϵ_c: (a), time spectrum obtained by the K x ray - K x ray coincidences; (b), integrated time spectrum. The coincidence efficiency $\epsilon_c \equiv N(\Delta t)/N$ has been deduced from the smoothed curve.

The values of the factors employed in Eq. (15) for the two separate measurements are listed in Table IV. The experimental value of the probability P_{KK} has been determined so to be

$$P_{KK}=(1.4\pm0.1)\times10^{-5}\,, \tag{18}$$

from weighted average of the two measurements.

For comparison, previous experimental P_{KK} values for ^{131}Cs and available theoretical predictions are summarized in Table V. The result of the measurement by Lark and Perlman[14] is considerably larger than the present result. This may have been caused by insufficient energy resolution of the x-ray detectors, i.e., NaI(T1) crystals; it is difficult to remove entirely the contribution of spurious events from this measured coincidence spectrum, e.g., coincidences between K x rays and IB photons and coincidences due to detector-to-detector scattering of one photon. Daniel, Schupp, and Jensen[34] did not take care of the spurious events, while the scrupulous elimination of such events resulted in a large statistical error in the P_{KK} value determined by Smith.[35]

The P_{KK} value of Nagy, Schupp, and Hurst (NSH) (Ref. 15) agrees with the present result within their statistical uncertainty. The higher precision of our result is due to improvements in the source preparation and detector resolution:

(i) The purification of the ^{131}Cs source is so complete that the Cs K x ray peak due to the contaminant ^{131}Ba, which was observed in previous measurements, does not appear in the present spectrum.

(ii) As seen in Fig. 2, the bumps of hypersatellite lines can be observed directly with the aid of the

TABLE IV. Data used for the determination of P_{KK}. Symbols defined in text.

	First measurement	Second measurement
ω_K[a]	0.904	0.904
N_H	1430±100	2560 ±150
ϵ_c	0.92±0.02	0.92±0.02
R_α	0.79±0.02	0.82±0.02
δ	$(1.53\pm0.07)10^8$	$(2.62\pm0.12)10^8$
P_{KK}	$(1.42\pm0.12)10^{-5}$	$(1.43\pm0.12)10^{-5}$

[a]Quoted from Ref. 27.

high-resolution pure Ge detector, while the Si(Li) detector used by NSH was not sufficient to resolve them from the diagram lines.

IV. DISCUSSION

Before comparing the present result with theoretical values calculated from various approaches, assumptions and approximations made in these approaches are summarized here in order to subsequently discuss the reliability of the numerical results in Table V. The atomic model used in previous approaches consists of a nucleus and a filled K shell. The model takes account of the correlation between two K shell electrons in the initial state, viz., the initial K-K correlation, ignoring any correlation effect between K shell and outer shell electrons. Then, in a complete description with nuclear and atomic variables, the matrix element for the K-EC decay is

$$M = \langle \psi_f^{Z-1} \psi_\nu \psi_f(N) \mid H_\beta \mid \psi_i(N) \psi_{KK}^Z \rangle , \quad (19)$$

where $\psi_i(N)$ and $\psi_f(N)$ are the initial and final nuclear wave functions, respectively, ψ_ν is the neutrino wave function, H_β is the weak-interaction Hamiltonian, ψ_{KK}^Z is the two-electron wave function of K shell electrons in the initial state, and ψ_f^{Z-1} is the final-state wave function of the uncaptured electron.

If the initial K-K correlation can be neglected, the separation between atomic and nuclear variables can be expressed as

$$M = \langle \psi_\nu \psi_f(N) \mid H_\beta \mid \psi_i(N) \psi_K^Z \rangle_{\text{nuclear}} \times \langle \psi_f^{Z-1} \mid \psi_K^Z \rangle_{\text{atomic}} , \quad (20)$$

where the first factor, containing only nuclear variables, represents the matrix element of the ordinary K-EC process, and the second factor, the atomic matrix element, is the overlap between initial and final electron states. However, as discussed by Carlson *et al.*,[36] calculations to determine such a simple overlap are no longer correct in the case where a sudden vacancy in a given shell promotes an additional electron ejection from the same shell. A many-body solution, explicitly containing electron-electron correlations, must be applied in the calculations. Actually, the main difficulty in calculating the P_{KK} value for K-EC decay consists of just how to take account of the initial K-K correlation in a theoretical formulation. This is why some unusual approximations were made in several previous approaches.

The importance of the initial K-K correlation is instructively shown in the nonrelativistic approach of Primakoff and Porter (PP),[4] where the approximation:

$$\psi_{KK} = N \psi_K^Z(r_1) \psi_K^2(r_2) \times \exp[\alpha \gamma_1 r_{12} + \alpha \gamma_2 (r_1 + r_2)] \quad (21)$$

was used as an initial-state two electron wave function. The function $\psi_K^Z(r)$ is a nonrelativistic $1s$ wave function, N is the normalization factor, and α is the hyperfine structure constant. The wave function given by Eq. (21) includes the effects of the mutual Coulomb interaction between two K electrons; the factor $e^{\alpha\gamma_2(r_1+r_2)}$ comes from the electrostatic shielding of the Coulomb attraction of the parent nucleus while the factor $e^{\alpha\gamma_1 r_{12}}$ describes the the effect of the spatial correlation between the two K electrons. In this calculation, the parameters γ_1 and γ_2 were chosen so that Eq. (21) becomes a good approximation to the variational wave function of Hylleraas for a two-electron atom: $\gamma_1 = 0.38$ and $\gamma_2 = 0.2$. Through a rough approximation, $P_{SO}(EC)$ is obtained as

TABLE V. Summary of experimental and theoretical results for ^{131}Cs.

Experimental $P_{KK}(\times 10^5)$	Theoretical P_{SO} and $P_{KK}(\times 10^5)$		
	P_{SO}	P_{KK}	
1.4±0.1 present work	~2.6[a]	3~4[b]	PP (Ref. 4)
5.0±1.0 Daniel *et al.* (Ref. 34)	0.92	*	Intemann (Ref. 7)
2.5±0.2 Lark and Perlman (Ref. 14)	3.38	3.53	LC (Ref. 10)[c]
2.0±1.3 Smith (Ref. 35)	0.71	1.79	MIKS (Ref. 13)
1.33±0.33 Nagy *et al.* (Ref. 15)		~7.0	Crasemann *et al.* (Ref. 38)

[a]Calculated from the rough approximation of Eq. (22).

[b]Calculated from the rough approximation of $P_{KK} \simeq \xi 0.18/Z^2$, where $\frac{1}{2} - \frac{2}{3}$ has been used as the multiplication factor ξ.

[c]See also Ref. 40 and addendum to discussion.

$$P_{SO}(EC) \simeq 0.08/Z^2 \quad (22)$$

for the total K-electron ejection (SO) probability per K-EC decay. This has to be compared with the same probability for the K-electron ejection during β^- decay, e.g.,

$$P_{SO}(\beta^-) \simeq 0.3/Z^2 \text{ per } K \text{ electron} , \quad (23)$$

which was derived from a nonrelativistic calculation[37] using the simple overlap as in Eq. (20). A notable decrease of $P_{SO}(EC)$ compared with $P_{SO}(\beta^-)$ indicates that the K-electron ejection during K-EC decay is much hindered by the initial K-K correlation.

Another evaluation has been given by Crasemann *et al.*[38] and concerns essentially the relative values of $1n$EC$-1'n'$SO events.

The absolute values predicted are too high, viz.,

$$P_{KK}(KEC-KSO) \sim 0.52Z^{-2,25} \text{per } KEC .$$

The overlap method based on the matrix element of Eq. (20) was employed by Stephas[12] and Mukoyama *et al.* (MIKS).[13] It was assumed in these approaches that the effect of the inital K-K correlation could be taken into account by adjusting the parameter in single-electron wave functions, i.e., the effective nuclear charge. This is clearly an oversimplification. Both total probabilities for K-electron shakeoff, P_{SO}, and for double K-hole creation, P_{KK}, were calculated by MIKS. The P_{SO} was derived using the matrix element of Eq. (20) and relativistic hydrogenic (RH) wave functions with the relativistic screening constant. The calculation for P_{KK} relies on a rather devious method based on the complete theorem

$$P_{SO}+P_{SU}+P_F+P_R=1 , \quad (24)$$

where P_{SU} is the probability for excitation of the uncaptured K electron to unoccupied shells (SU) and P_F is the probability of excitation to occupied shells, which are forbidden by the Pauli principle, P_R is the probability for the K electron remaining in the K shell. Then P_{KK} is given by

$$P_{KK}(\equiv P_{SO}+P_{SU}) = 1-P_F-P_R ,$$
$$= \xi(1-P_R) , \quad (25)$$

where the multiplicative factor was defined as

$$\xi = \frac{1-(P_F)_{\text{many}-e}-(P_R)_{\text{many}-e}}{1-(P_R)_{\text{many}-e}} . \quad (26)$$

The probability P_R in Eq. (25) was calculated according to the same formulation as for P_{SO}. The probabilities $(P_F)_{\text{many}-e}$ and $(P_R)_{\text{many}-e}$ for the factor ξ were calculated using a nonrelativistic self-consistent-field (SCF) wave function of Herman and Skillman.[39] It should be noted that the RH wave functions with screening constant are no longer orthogonal. This nonorthogonality (or near orthogonality) makes the overlap integral very sensitive to the exact form of the wave function and therefore to the value chosen for the effective charge. The accuracy of these numerical results may not be very reliable. The big difference between P_{KK} and P_{SO} values in Table V indicates that there may be some inconsistency in this theoretical formulation. In spite of not-evident approximations in MIKS's formulation, the difference between the present experimental P_{KK} and their P_{KK} is unexpectedly small.

A different approach, which is free from adjustable parameters, was developed by Intemann[5,7] and independently by Law and Campbell (LC).[10] It was assumed in these approaches that the initial K-K correlation can be treated as a perturbation along with the weak interaction, with the result that such a correlation should be, in principle, included in the unperturbed Hamiltonian as in the approach by PP. Intemann expressed the matrix element of Eq. (19) using the Coulomb Green's functions similar to those of the theory of internal bremsstrahlung (IB) accompanying EC decay.[6] In his relativistic calculation, he employed the solution of the symmetric Hamiltonian of Biedenharn and Swamy[9] for the Coulomb Green's functions, which differs from the exact Dirac-Coulomb eigenfunctions by terms of order $(\alpha Z)^2$. His calculations were much simplified owing to the closed form of the approximate Green's function. As proved by Intemann,[8] this approach is identical with that of LC. A difference in their formulation is that LC used the Coulomb Green's function expressed in the form of eigenfunction expansion while Intemann used the function in the closed form. The large discrepancy between numerical results by Intemann and those by LC has been explained by the fact that LC cut off the eigenfunction expansion too soon.[8]

Thus, the most consistent prediction in Table V is due to Intemann. Possible sources for the definite difference between the present experimental P_{KK} and his theoretical P_{SO} are the following:

(i) The SU probability, P_{SU}, is to be added to the P_{SO} value although the P_{SU} is expected to be small compared with the P_{SO}.

(ii) The approximation for the Coulomb Green's function in the closed form may have a nonnegligible influence on his P_{SO} value.

(iii) The initial K-K correlation is assumed to be a perturbation in his approach. Since such a correlation is generally too large to be treated as a perturbation, this assumption may introduce a nonnegligible error.

(iv) The effect of the many-body correlation between K-shell and outer shell electrons are neglected.

It is difficult to discuss the magnitude of errors to be expected from the possible sources (i)—(iv). Further calculations according to the formulation by LC are desirable, because the P_{SO} by the LC formulation will be free from approximation (ii) and the estimation of P_{SU} may be straightforward. A comparison of the present experimental result with the the P_{KK} thus evaluated will solve basic questions stemming from sources (iii) and (iv).

[*Note added.* We have learned very recently about new calculations by Suzuki and Law (SL) (Ref. 40) who use a SCF method to evaluate the $P(K\text{SO})$ value, taking account of initial state K-K correlation and of screening in the final state. For ^{131}Cs, the result, 3.2×10^{-5}, remains larger than the present experimental value. SL observe the high sensitivity of the calculated value as regarding the adjustable parameter γ, interpreted as an effective charge stemming from the initial state residual correlation. This point is under further examination as well as improved calculations of the continuum final state.]

In summary, the double K-hole creation probability P_{KK} in the EC decay of ^{131}Cs has been measured with good precision; $P_{KK}=(1.4\pm0.1)\times10^{-5}$ per K-EC decay. A refined calculation for P_{KK} is clearly required. The α_1^H/α_2^H ratio has been determined to be 1.5 ± 0.2 by the aid of a nonlinear least-squares fit with appropriate constraints. The measured ratio agrees with recent predictions. The intensity of ^1s IB photons in the decay of ^{131}Cs has been reevaluated: $P_{IB}(^1s)=(2.5\pm0.7)\times10^{-5}$ per K-EC decay. The present work has shown that, with a careful K x ray $\otimes$ K x ray coincidence measurement, a P_{KK} value can be obtained precise enough to be compared with theory. Refined measurements with ^{55}Fe, ^{71}Ge, and ^{165}Er, which can also be purified just as completely as ^{131}Cs, are desirable to obtain more reliable experimental P_{KK} values.

ACKNOWLEDGMENTS

The authors wish to express their sincere thanks to Dr. P. Magnier (Laboratoire de Métrologie des Rayonnements Ionisants, CEN Saclay) for calibrating our ^{131}Cs sources to a high degree of precision. The invaluable help of Dr. J. P. Thibaud is acknowledged. One of us (Y.I.) expresses his sincere thanks to Professor S. Shimizu for continual encouragement.

---

*Experiment carried out during sabbatical leave at the Laboratoire de Spectrométrie Nucléaire, Orsay, France.

[1]M. S. Freedman, Annu. Rev. Nucl. Sci. 24, 209 (1974).

[2]R. J. Walen and Ch. Briançon, in *Atomic Inner-shell Processes,* edited by B. Crasemann (Academic, New York, 1975), Vol. 1, p. 233.

[3]W. Bambynek, H. Behrens, M. H. Chen, B. Crasemann, M. L. Fitzpatrick, K. W. D. Ledingham, H. Genz, M. Mutterer, and R. L. Intemann, Rev. Mod. Phys. 49, 77 (1977).

[4]H. Primakoff and F. T. Porter, Phys. Rev. 89, 930 (1953).

[5]R. L. Intemann and F. Pollock, Phys. Rev. 157, 41 (1967).

[6]R. J. Glauber and P. C. Martin, Phys. Rev. 104, 158 (1956); 109, 1037 (1958).

[7]R. L. Intemann, Phys. Rev. 178, 1543 (1969); 188, 1963 (1969); Phys. Rev. C 3, 1 (1971); 6, 211 (1972).

[8]R. L. Intemann, Nucl. Phys. A219, 20 (1974).

[9]L. C. Biedenharn and N. V. V. J. Swamy, Phys. Rev. 133, B1353 (1964).

[1]J. Law and J. L. Campbell, Nucl. Phys. A199, 481 (1973).

[11]G. Paquette, Can. J. Phys. 40, 1765 (1962).

[12]P. Stephas, Phys. Rev. 186, 1013 (1969).

[13]T. Mukoyama, Y. Isozumi, T. Kitahara, and S. Shimizu, Phys. Rev. C 8, 1308 (1973).

[14]N. L. Lark and M. L. Perlman, Phys. Rev. 120, 536 (1960).

[15]H. J. Nagy, G. Schupp, and R. R. Hurst, Phys. Rev. C 6, 607 (1972).

[16]W. von Oertzen, Z. Phys. 182, 130 (1964).

[17]J. P. Briand, P. Chevallier, M. Tavernier, and J. P. Rozet, Phys. Rev. Lett. 27, 777 (1971).

[18]C. W. E. van Eijk, J. Wijnhorst, and M. A. Popelier, Phys. Rev. C 19, 1047 (1979); 20, 1749 (1979).

[19]H. Ryde, L. Person, and K. Oelsner-Ryde, Ark. Fys. 23, 171 (1963).

[20]Z. Sujkowski, B. Myslek, J. Lukasiak, and B.

Kotlinska-Filipek, U.S. AEC Report No. CONF-720404, 1973 (unpublished), Vol. 3, p. 2005.
[21]M. Mutterer, U.S. AEC Report No. CONF-701002, 1970 (unpublished), p. 452.
[22]J. G. Pengra and B. Crasemann, Phys. Rev. 131, 2642 (1963).
[23]H. J. Nagy, ATOMKI Kozl. 13, 101 (1971).
[24]T. Kitahara and S. Shimizu, Phys. Rev. C 11, 920 (1975).
[25]W. Neumann, Proceedings of the International Conference on x-ray Processes and Inner Shell Ionization, Stirling, 1980.
[26]S. Bjornholm, E. R. Johansen, and H. Nordby, Nucl. Instrum. Methods 27, 243 (1963).
[27]V. O. Kostroun, M. H. Chen, and B. Crasemann, Phys. Rev. A 3, 533 (1971).
[28]J. H. Scofield, in *Atomic Inner-shell Processes,* edited by B. Crasemann (Academic, New York, 1975), Vol. 1, p. 265.
[29]M. H. Biavati, S. J. Nassiff, and C. S. Wu, Phys. Rev. 125, 1364 (1962).
[30]J. P. Desclaux, Comput. Phys. Commun. 9, 31 (1975).
[31]Ch. Briançon and J. P. Desclaux, Phys. Rev. A 13, 2157 (1976).
[32]T. Åberg, J. P. Briand, P. Chevallier, A. Chetioui, J. P. Rozet, M. Tavernier, and A. Touati, J. Phys. B 9, 2815 (1976).
[33]T. Åberg and M. Suvanen, in *Advances in x-ray Spectroscopy,* edited by C. Bonnelle and C. Maude (Pergamon, New York, 1981).
[34]H. Daniel, G. Schupp, and E. N. Jensen, Phys. Rev. 117, 823 (1960).
[35]K. M. Smith, Ph.D. thesis, University of Glasgow, 1964 (unpublished).
[36]T. A. Carlson, C. W. Nestor, Jr., T. C. Tucker, and F. B. Malik, Phys. Rev. 169, 27 (1968).
[37]E. L. Feinberg, J. Phys. (U.S.S.R.) 4, 423 (1941).
[38]B. Crasemann, M. H. Chen, J. P. Briand, P. Chevallier, A. Chetioui, and M. Tavernier, Phys. Rev. C 19, 1042 (1979).
[39]F. Herman and S. Skillman, *Atomic Structure Calculations* (Prentice-Hall, Englewood Cliffs, 1963).
[40]A. Suzuki and J. Law. Phys. Rev. C. 25, 2722 (1982); private communication.